Reactive and Functional Polymers 125 (2018) 57–69

Contents lists available at ScienceDirect

Reactive and Functional Polymers

journal homepage: www.elsevier.com/locate/react

Optimized formulation of $NiFe_2O_4$@Ca-alginate composite as a selective and magnetic adsorbent for cationic dyes: Experimental and modeling study

Corneliu Cojocaru*, Andra Cristina Humelnicu, Petrisor Samoila, Petronela Pascariu, Valeria Harabagiu

"Petru Poni" Institute of Macromolecular Chemistry, Aleea Grigore Ghica Voda 41A, 700487 Iasi, Romania

ARTICLE INFO

Keywords:
Alginate
Spinel ferrite
Dye adsorption
Modeling and optimization
Molecular docking simulation

ABSTRACT

This paper reports a data-driven modeling methodology undertaken to establish the optimal formulation of $NiFe_2O_4$@Ca-alginate composite designed for adsorption applications. Adsorbents were produced as anisotropic plate-like particles that were applied for removal of Rhodamine-6G (Rh6G) and Methylene Blue (MB) cationic dyes from aqueous solutions. Data-driven models were developed to establish the composition-performance relationships and to optimize the formulation of the composite adsorbent. The optimal formulation of $NiFe_2O_4$@Ca-alginate composite implied a content of 16% (w/w) $NiFe_2O_4$ nanoparticles into the alginate matrix. Likewise, kinetics, isotherms and thermodynamics studies were carried out and reported in this paper. The optimal adsorbent ($NiFe_2O_4$@Ca-alginate) yielded a remarkable maximal sorption capacity equal to 1243 mg/g (for MB uptake) and 845 mg/g (for Rh6G) at the room temperature (298 K). Dubinin-Radushkevich (D-R) isotherms revealed the mean free energy of sorption ranging from 7.23 to 9.26 (kJ/mol) suggesting that the mechanism of adsorption was based on both physical interactions and ion exchange. This evidence was also corroborated by the molecular docking simulations that highlighted valuable insights regarding the intermolecular interactions between alginate chains and cationic dyes.

1. Introduction

Synthetic dyes are complex organic molecules designed to be chemically stable compounds [1]. Both synthetic and natural dyes are generally recalcitrant to biodegradation [2]. Therefore, water pollution with dyes represents a serious environmental problem owing to the persistence and toxicity of these organic contaminants. Likewise, the discharge of colored effluents into aquatic ecosystems can diminish the sunlight penetration and photosynthesis [3].

The main activities involved in the discharge of dyes into waterways are related to the conventional industries such as textile, leather, rubber, cosmetic, paper, plastic, pharmaceutical, photographic and food-processing [1,3]. For instance, the Rhodamine 6G (Rh6G) dye represents a cationic dye widely used in acrylic, nylon, silk, and wool coloring technologies [2].

Typically, dye wastewaters are treated by various physical, chemical and biological methods such as advanced oxidation, electrochemical treatment, coagulation-flocculation, aerobic or anaerobic processes, membrane separations and adsorption [1,3,4]. All these methods have particular advantages and limitations. However, the adsorption is considered to be the most preferable technique in terms of simplicity of design, initial cost, facile operation and low energy requirements [5]. Hence, the adsorption has gained importance as a feasible purification and separation technique used in water and wastewater treatment.

So far, a wide variety of sorbent materials was used for dyes removal from wastewaters, such as activated carbon [6,7], inorganic products [8,9], polymeric resins [10–12] and low-cost materials [13–22] mainly derived from the naturally abundant biomass and solid wastes. Likewise, biopolymers such as chitosan and alginate proved high performances for the removal of anionic and cationic dyes, respectively [23–31]. In spite of their efficient adsorption abilities, the main disadvantage of conventional sorbents is related to the separation inconvenience that requires an additional filtration step. In this respect, the development of new multifunctional adsorbents has attracted a great interest within the perspective of the sustainable development [32]. Hence, the formulation of the composite adsorbents aims to produce multifunctional materials with relevant adsorption performance, mechanical resistance, selectivity and suitable magnetic properties for a facile separation.

In the last decades, alginate-based adsorbents and composites were mostly produced as beads tailored for the removal of cationic dyes and

* Corresponding author.
E-mail address: cojocaru.corneliu@icmpp.ro (C. Cojocaru).

https://doi.org/10.1016/j.reactfunctpolym.2018.02.008
Received 28 November 2017; Received in revised form 12 February 2018; Accepted 13 February 2018
Available online 14 February 2018
1381-5148/

heavy metal ions from wastewaters [27–39]. The good adsorption capacity of alginate-based materials is explained by their binding with cationic species owing to the content of carboxylic groups.

So far, various alginate-based composites were developed as adsorbents for cationic dyes removal; for example, alginate-cellulosic residue (vineyard pruning waste) biocomposites [32,33]; montmorillonite/alginate [3,34]; alginate/titania nanoparticles [35]; graphene/alginate [36]; graphene oxide/calcium alginate [37] and magnetic alginate beads [38,39]. The alginate-based materials produced as beads may be used as appropriate adsorbents for dynamic mode (fixed-bed/column) applications. This is because the beads of several millimeters in size can be properly packed into a column to ensure a good hydrodynamic flow. However, for the batch mode adsorption, it may seem that sorbents in the form of sub-millimeter particles might be more efficient due to higher contact surface-area comparing to the conventional beads.

The main objective of this work was to develop alginate-based magnetic composites as sub-millimeter particles for batch adsorption applications and to facilitate their magnetic separation after usage. Specific objectives involved the design of experiments for the formulation of composites; data-driven modeling and process optimization; as well as molecular docking simulations to gain more insights about interaction mechanism. Herein, we employed Rhodamine 6G (Rh6G) as the main model dye pollutant because of its rigid structure, refractory character [40] and remarkable photo-stability. In addition, the cationic dye Methylene Blue (MB) was also used in adsorption tests for comparison.

2. Materials and methods

2.1. Materials

Analytical grade $Ni(NO_3)_2{\cdot}6H_2O$, $Fe(NO_3)_3{\cdot}9H_2O$, citric acid monohydrate, Rhodamine 6G (Rh6G) and Methylene Blue (MB) cationic dyes were purchased from Sigma-Aldrich and used without further purification. The alginic acid sodium salt was also acquired from Sigma-Aldrich with the following product specification: 1) the molecular weight of 120,000–190,000 g/mol; 2) the ratio of mannuronic acid to guluronic acid (M/G ratio) equal to 1.56, and 3) viscosity of 15–20 cPs for the solution of 1% w/w sodium alginate in water.

2.2. Preparation of $NiFe_2O_4$ magnetic component

First, $NiFe_2O_4$ spinel ferrite was prepared by the sol-gel auto-combustion method [41]. In this experiment, stoichiometric amounts of metal nitrates were dissolved in distilled water with a molar ratio Ni^{2+}/Fe^{3+} of 1:2. Second, an aqueous solution of citric acid was prepared taking into account 1:1 M ratio of citric acid to metal cations. Third, the citric acid solution was added to the solution of nitrate salts and heated to 80 °C on a water bath, under stirring until a viscous gel was formed. The gel was gradually heated to 350 °C to promote the auto-ignition process. The resulting powder was sintered in two steps (at 500 °C/5 h and at 700 °C/5 h) to yield the spinel-phase formation.

2.3. Preparation of $NiFe_2O_4$@Ca-alginate composites

Alginate solutions of 2–3% (w/w) concentration were prepared by dissolving designed amounts of sodium alginate in distilled water at 30 °C under magnetic stirring. All alginate aqueous solutions were subjected to ultrasonication for 30 min and left overnight to reach the thermodynamic equilibrium. The casting solutions used for producing of composite membranes were prepared by mixing 30 mL of sodium alginate solution and 10 mL ferrofluid containing $NiFe_2O_4$ nanoparticles (1–3% w/v) dispersed in distilled water under ultrasonication. The ferrofluid was added slowly into sodium alginate solution, and the mixture was subjected to ultrasonic vibrations for 45 min. The resulted mixture was poured into Petri dishes, and the casting solution was dried at 40 °C for 24 h to allow the solvent evaporation. Note that, the added amount of spinel ferrite into the ferrofluid (i.e., 1 to 3% w/v) was designed in such way to yield a content of 15–25% w/w $NiFe_2O_4$ into the final solid-phase of composite. The dried composite membranes were weighted and left for 48 h into a desiccator. Finally, the membranes were post-treated using calcium chloride solutions (0.05–0.15 M) as ionic cross-linking agents. To this end, the composite membranes were immersed for 1 h in $CaCl_2$ solution, followed by washing with distilled water five times and drying for 24 h at 30 °C.The resulted cross-linked membranes were cut and ground using a laboratory mill (IKA A10 basic). Finally, the resulted chopped shreds were sieved (using a mesh with 0.84 mm openings) to obtain the adsorbent in the form of sub-millimeter particles.

2.4. Characterization techniques

The surface morphology of the produced composite adsorbents was investigated by scanning electron microscopy (SEM) using an (ESCM) Quanta 200 device equipped with Energy Dispersive X-ray (EDX) system. The SEM images were examined by ImageJ open-source software for scientific image analysis.

Infrared absorption spectra (FTIR) of materials were recorded within the range 400–4000 cm^{-1} with a resolution of 2 cm^{-1} by using a Bruker Vertex 70 FTIR spectrometer.

Magnetic measurements on the composite (alginate/$NiFe_2O_4$) were done using an MPMS3 (7 T) SQUID magnetometer, at room temperature (300 K), in DC mode. Before each measurement, the sample was AF (alternating field) demagnetized.

2.5. Adsorption experiments

To carry out adsorption experiments, first, a stock solution of 1000 mg/L concentration was prepared by dissolving the cationic dye in distilled water. The concentrated stock solution was used to produce working solutions by the dilution technique. The concentrations of dye in the initial and post-adsorption solutions were analyzed by monitoring the absorbance on a UV–Vis spectrophotometer (Shimadzu UV-1700 PharmaSpec). In this respect, Rh6G and MB dyes were monitored at 526 nm and 668 nm wavelengths, respectively. The composite adsorbents were tested for the removal of cationic dyes from aqueous solutions in the batch adsorption mode. To this end, designed amounts of adsorbents were added to 50 mL of working solutions (in Erlenmeyer flasks), and the samples were stirred at 240 rpm using an environmental shaker incubator (BIOSAN ES-20/60) equipped with a system for temperature control. All adsorption experiments were carried out at pH 6.5 ± 0.2, excepting the study related to pH influence. At the end of each adsorption test, the spent adsorbent was separated using an external magnet, and the resulted purified solution was analyzed for the dye content.

In all experiments (i.e. design optimization, kinetics and isotherms) the adsorption capacity was determined as given by:

$$q = \frac{(C_0 - C)\cdot V}{m\cdot 1000} \quad (1)$$

where q denotes the adsorption capacity (mg/g); C_0 is the initial concentration of dye (mg/L); C is the final concentration of dye (mg/L); V is the volume of solution (mL) and m represents the weight of the adsorbent (g).Likewise, the color removal efficiency Y (%) was calculated as:

$$Y = \left(1 - \frac{C}{C_0}\right) \times 100 \quad (2)$$

3. Results and discussion

3.1. Design of experiments for the formulation of composite adsorbents

The spinel ferrite ($NiFe_2O_4$) produced by auto-combustion method was employed as a magnetic component for the formulation of the alginate-based composite adsorbents. The main characteristics of nickel spinel ferrite ($NiFe_2O_4$) were detailed in our previous paper [41]. Briefly, the maximal peak identified in the X-ray diffraction pattern (at $2\theta = 35.7^{\circ}$) corresponded to the face-centered cubic structure of pure spinel, according to JCPDS card number 44-1485. The crystallite size of $NiFe_2O_4$ ascertained from XRD pattern was equal to 30.6 nm. In addition, the average particle size of 46 nm was determined from the transmission-electron-microscopy images (TEM). The infrared spectrum of $NiFe_2O_4$ (FTIR, not shown here) unveiled only two peaks, i.e. 584 cm^{-1} attributed to metal-oxygen stretching vibration from the tetrahedral site and at 397 cm^{-1} assigned to metal-oxygen stretching from the octahedral site [41].

Subsequently, $NiFe_2O_4$@Ca-alginate composite adsorbents were prepared as detailed in the experimental Section 2.3. The controllable input variables (factors) considered for the formulation of composites were as follows: 1) sodium alginate concentration in aqueous solution (z_A, 2–3% w/w); 2) content of $NiFe_2O_4$ within the composite solid phase, (z_F, 15–25% w/w); 3) $CaCl_2$ concentration in post cross-linking bath, (z_I, 0.05–0.15 M). For modeling purpose, these factors were also converted into coded variables (x_1, x_2 and x_3) ranging from −1 to +1 (Table 1).

A central-composite design of face-centered type (Table 2) was adopted for the fabrication of composite adsorbents summarizing all preparation conditions (17 runs).The produced alginate-based composites according to each run were designated as AC1 to AC17, respectively. Note that, samples AC15, AC16 and AC17 were prepared under the same conditions (runs 15–17) to test the reproducibility of the experiment.

Hence, the compositional diversity of $NiFe_2O_4$@Ca-alginate adsorbents (AC1-AC17) was achieved by varying the concentration of sodium alginate, the content of spinel ferrite and the concentration of $CaCl_2$ in the post cross-linking bath. Fig. 1 reports a SEM image showing the particles morphology and size as well as their size distribution (histogram) determined for the adsorbent sample AC1 (as an example). According to Fig. 1, the adsorbent sample involves irregular plate-like particles with the size ranging from 90 μm to 1180 μm, and an average size of 485 μm. Similar particle size distributions were observed and for the other samples. Each developed composite material (AC1 to AC17) was tested for the adsorption of Rh6G dye from aqueous solutions using the following conditions:50 mg/L (C_0, initial dye concentration), 2 g/L (*SD*, sorbent dosage), 25 °C and pH 6.5 ± 0.2. Accordingly, the adsorption performances (responses) of each produced composite material were determined in terms of *adsorption capacity* (q, mg/g) and *color removal efficiency* (Y, %). Observed values of both responses (q and Y) are also summarized in Table 2.

Table 1
Design variables and their coded and actual values used for experimentation.

Design variables (factors)	Coded variables	Coded levels versus actual values		
		−1	0	+1
Concentration of sodium alginate in precursor aqueous solution, z_A (% w/w)	x_1	2.0	2.5	3.0
Content (dosage) of $NiFe_2O_4$ within the composite solid phase, z_F (% w/w)	x_2	15.0	20.0	25.0
Concentration of $CaCl_2$ in post cross-linking solution, z_I (M)	x_3	0.05	0.10	0.15

Table 2
Central composite design used for adsorbents preparation and their testing for Rh6G uptake.

Run	Factors (controllable input variables)						Composite adsorbent	Responses	
	Sodium Alginate		$NiFe_2O_4$		$CaCl_2$				
	x_1	z_A (% w/w)	x_2	z_F, (% w/w)	x_3	z_I (M)	Material code	q (mg/g)	Y (%)
1	+1	3.0	+1	25.0	+1	0.15	AC1	12.406	49.140
2	−1	2.0	+1	25.0	+1	0.15	AC2	12.848	47.726
3	+1	3.0	−1	15.0	+1	0.15	AC3	14.185	53.814
4	−1	2.0	−1	15.0	+1	0.15	AC4	14.096	53.440
5	+1	3.0	+1	25.0	−1	0.05	AC5	19.400	75.700
6	−1	2.0	+1	25.0	−1	0.05	AC6	17.266	65.401
7	+1	3.0	−1	15.0	−1	0.05	AC7	19.506	77.086
8	−1	2.0	−1	15.0	−1	0.05	AC8	17.142	65.160
9	+1	3.0	0	20.0	0	0.10	AC9	18.844	71.277
10	−1	2.0	0	20.0	0	0.10	AC10	16.602	61.562
11	0	2.5	+1	25.0	0	0.10	AC11	17.347	67.800
12	0	2.5	−1	15.0	0	0.10	AC12	18.516	71.825
13	0	2.5	0	20.0	+1	0.15	AC13	14.754	54.735
14	0	2.5	0	20.0	−1	0.05	AC14	19.278	73.891
15	0	2.5	0	20.0	0	0.10	AC15	18.232	68.821
16	0	2.5	0	20.0	0	0.10	AC16	18.356	69.497
17	0	2.5	0	20.0	0	0.10	AC17	18.291	69.153

3.2. Multiple regression modeling

On the basis of the experimental design and collected data reported in Table 2, two mathematical models were developed using the multiple regression method and response surface methodology [42–44]. These fitting models establish the relationships between adsorption responses (q and Y) and the input controllable factors. The modeling equations in terms of coded variables are given by:

$$\hat{q} = 18.34 + 0.64x_1 - 0.42x_2 - 2.43x_3 - 0.66x_1^2 - 0.45x_2^2 - 1.37x_3^2 - 0.61x_1x_3 - 0.38x_2x_3 \quad (3)$$

$$\hat{Y} = 69.46 + 3.37x_1 - 1.57x_2 - 9.84x_3 - 3.27x_1^2 - 5.38x_3^2 - 2.55x_1x_3 - 1.16x_2x_3 \quad (4)$$

subject to: $x_i \in [-1, +1]$; $\forall\, i = \overline{1,3}$where x_1, x_2 and x_3 denote the coded input variables; $\hat{q}$ and $\hat{Y}$are the predicted adsorption capacity and color removal efficiency, respectively.

Multiple regression equations (Eqs (3) and (4)) represent second-order models with interaction terms, implying significant coefficients. In addition, models were statistically validated by the analysis of variance (ANOVA) [42–44]. Statistical summaries (ANOVA) are reported in the *electronic supporting information* (*ESI*) section, in Tables S1 and S2. According to ANOVA results (Tables S1–S2), the probability values (*p-value)* were < 0.0001, and the determination coefficient (R^2) was close to unity. Therefore, the developed models were significant for exploring the design space. The agreements between predicted and observed responses are shown in Fig. 2. As can be seen, both models are in good agreement with experimental observations. In summary, the parity plots (Fig. 2) along with ANOVA outcomes corroborated the goodness-of-fit. Final empirical models in terms of actual variables can be written as:

$$\hat{q} = -16.62 + 16.90z_A + 0.79z_F + 151.85z_I - 2.64z_A^2 - 0.02z_F^2 - 546.82z_I^2 - 24.26z_Az_I - 1.52z_Fz_I \quad (5)$$

$$\hat{Y} = -59.48 + 83.34z_A + 0.15z_F + 581.16z_I - 13.08z_A^2 - 2.15 \times 10^3 z_I^2 - 102.18z_Az_I - 4.62z_Fz_I \quad (6)$$

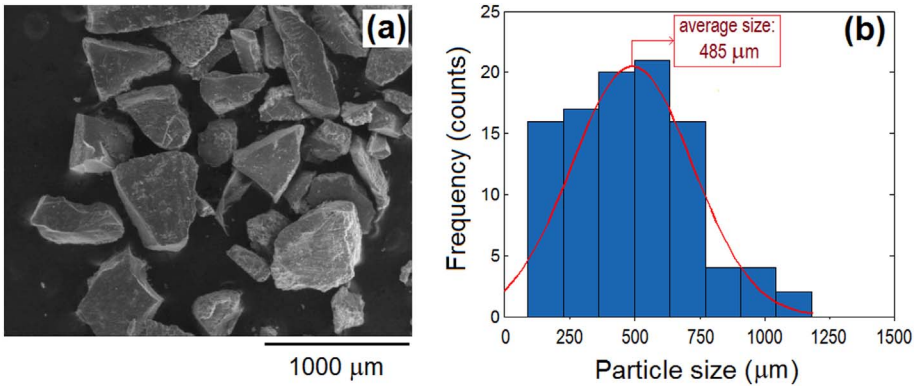

Fig. 1. Particle size and distribution for the composite adsorbent (AC1 sample): (a) SEM image of the composite adsorbent particles; (b) histogram of particle size distribution.

subject to:$2.0 \le z_A \le 3.0$ (% w/w); $15.0 \le z_F \le 25.0$ (% w/w); $0.05 \le z_I \le 0.15$ Mwhere z_A denotes the alginate concentration in aqueous solution; z_F – content of ferrite in the composite solid phase, and z_I – concentration of Ca^{2+} in the post-crosslinking bath.

Subsequently, computer-aided simulations were performed based on empirical models (Eqs (5)–(6)) to render adsorption performances as functions of input variables. Hence, Figs. 3–4 show the coupling effects of factors (z_A, z_F and z_I) on the adsorption responses ($\hat{q}$ and $\hat{Y}$). Note that, each factors' combination (z_A, z_F and z_I) represents a material formulation, which is inherently connected to the material performance ($\hat{q}$ and $\hat{Y}$) as detailed by response surface graphs (Figs. 3–4).

Fig. 3 illustrates the combined effects of z_A (alginate), z_F (ferrite) and z_I ($CaCl_2$) input variables on the adsorption capacity ($\hat{q}$). According to Fig. 3a, contributions of z_A and z_F factors are comparable as magnitude. These imply the main and quadratic effects of both factors to the adsorption performance ($\hat{q}$). The response surface analysis indicated that with the increment of the alginate content in the composite, the adsorption capacity is improved. In contrast, the greater the ferrite content, the less adsorption capacity is (Fig. 3a). There is no interaction effect between z_A (alginate) and z_F (ferrite) factors. According to Fig. 3b, the influence of z_I ($CaCl_2$) factor is much greater than the effect of the ferrite (z_F), and respectively, of the alginate (z_A). The less the factor z_I ($CaCl_2$), the greater is the adsorption capacity ($\hat{q}$) of the resulted material. In other words, dilute solutions of $CaCl_2$ in the post-treatment bath yielded a better adsorption performance of the produced cross-linking materials. Note that, a small interaction effect can be perceived between z_F (ferrite) and z_I ($CaCl_2$) factors from Fig. 3b. This suggests that the influence of z_I ($CaCl_2$) is of less importance for the alginate-based composites with lower content of the magnetic component ($NiFe_2O_4$).

The relationship between the color removal efficiency ($\hat{Y}$) and input factors is depicted in Fig. 4. As one can see, the increment of alginate content (z_A) in the composite matrix improves the color removal efficiency (Fig. 4a). By contrast, the greater the variables z_F and z_I, the less is the color removal efficiency (Fig. 4a–b). According to the response surface analysis, the concentration of calcium chloride (z_I) is the most significant factor, whereas the alginate content in the composite matrix is a factor of secondary importance. By contrast, the ferrite content is the least significant variable affecting the color removal efficiency. From Fig. 4a–b, one may observe curvature shapes of the response surface accounting for strong and moderate quadratic effects of the z_I and z_A factors, respectively. Likewise, an interaction effect between z_I and z_A input variables can be noticed from Fig. 4b, revealing that the influence of z_I ($CaCl_2$) factor is stronger for a composite material with higher content of alginate (z_A).

3.3. Optimization by desirability function approach

One purpose of this study was to optimize the formulation of the alginate-based composite to achieve the most efficient magnetic adsorbent for cationic dyes removal. To this end, we employed the response surface analysis and desirability function approach. First, we identified the desirability region (near-to-optimum) by visual inspection of the overlap contour-lines maps as shown in Fig. 5. Herein, the overlay of both response functions $\hat{q}$ and $\hat{Y}$ is detailed. Note that, Fig. 5 presents overlap contour-line maps for the factorial space z_A (alginate) and z_F (ferrite) at fixed levels of the third variable ($CaCl_2$), i.e. $z_I = 0.1$ M (see Fig. 5a) and $z_I = 0.05$ M (see Fig. 5b). It turns out from Fig. 5 that $\hat{q}$ and $\hat{Y}$ response functions are not obviously conflicting. For instance, with increasing of z_A and decreasing of z_F variables, both responses are improved. As one can see, the contour-lines profile at $z_I = 0.1$ (Fig. 5a) is different from the one calculated at $z_I = 0.05$ (Fig. 5b). Curvatures of both response functions ($\hat{q}$ and $\hat{Y}$) are clearly observed in the first case (Fig. 5a). By contrast, the curvature of $\hat{Y}$ response is dramatically reduced for the second case (see Fig. 5b). More precisely, straight contour-lines and respectively a linear behavior

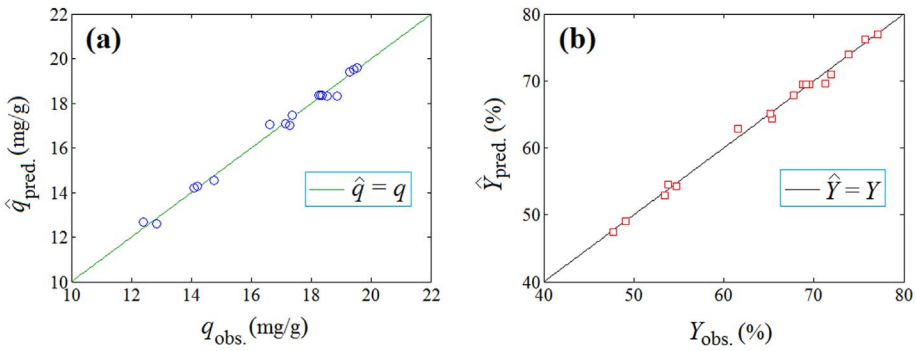

Fig. 2. Agreements between experimental observations of responses and their predictions provided by fitted models: (a) goodness-of-fit for adsorption capacity; (b) goodness-of-fit for color removal efficiency; (adsorptive removal of Rh6G dye).

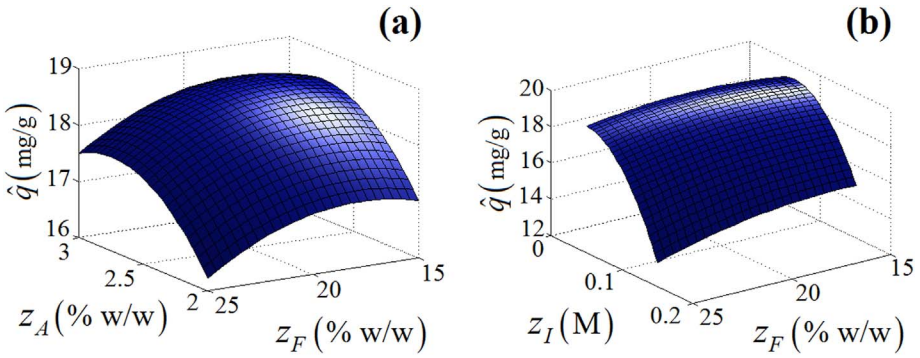

Fig. 3. Response surface plots showing the coupling effects of factors on the adsorption capacity (adsorption of Rh6G dye):(a) effects of factors z_A and z_F (at z_I = 0.1 M); (b) effects of factors z_I and z_F (at z_A = 2.5% w/w).

of the output function $\hat{Y}$ can be discerned from Fig. 5b. Herein, the desirability zone (green-colored) was identified for the restricted domain given by the following constraints $2.6 \le z_A \le 3.0$ and $15 \le z_F \le 17$. This region indicated higher values of both responses (Fig. 5b).

Next step was to perform the multi-objective optimization by using *desirability function approach* (DFA). In accordance with this method, actual values of output functions (responses) must be converted into normalized *individual desirability functions* (*d*) ranging from 0 to 1 (e.g. $\hat{q} \rightarrow d_q$ and $\hat{Y} \rightarrow d_Y$). To this end, we applied the conversion scheme of LTB type (the-larger-the-best), because maximal values of both responses ($\hat{q}$ and $\hat{Y}$) were of interest. Details regarding the LTB-type conversion scheme can be found within the literature [44,45]. Finally, the individual desirability functions (d_q and d_Y) were merged into a composite function, known as the *global desirability* (*D*) that was expressed as the geometrical mean between components [44,45]:

$$D = \sqrt{d_q \times d_Y} \tag{7}$$

Basically, the overall desirability *D* must be maximized to find optimum conditions that ensure the greatest values of adsorption responses $\hat{q}$ and $\hat{Y}$. Hence, the multi-objective optimization problem was addressed by desirability function approach coupled with Monte-Carlo stochastic method [46]. The equivalent optimal solutions, revealing the highest values of global desirability ($D > 0.87$), are reported in Table S3 (*ESI*). These equivalent points corresponded to three new produced adsorbents designated as AC18, AC19 and AC20. The preparation conditions for all of them implied a high content of alginate and low concentration of calcium chloride. The distinction between these composites relied on the different content of $NiFe_2O_4$ (16–19%) as detailed in Table S3 (*ESI*).To decide the best adsorbent from AC18, AC19 and AC20 samples, the confirmation runs (experimental validation) were performed (see Table S3). On the basis of observations, the AC20 composite was decided as the ultimate optimal adsorbent. Note that, the AC20 composite prepared under conditions of 3% (alginate), 16% ($NiFe_2O_4$) and 0.05 M ($CaCl_2$) yielded the greatest observed desirability value of 0.886 owing to the highest adsorption performances, i.e. q = 19.52 mg/g and Y = 78.81%. Therefore, the alginate-based adsorbent AC20 was retained for the next experimental studies owing to its optimal formulation.

3.4. Characteristics of the optimal composite adsorbent ($NiFe_2O_4$@Ca-alginate)

The optimal alginate-based magnetic adsorbent (AC20 sample) was characterized in terms of surface morphology (SEM-EDX), infrared spectrometry and magnetic measurements.

Fig. 6 gives the hysteresis loop plot for the composite ($NiFe_2O_4$@Ca-alginate) measured at room temperature with maximum applied field of 4KOe. The hysteresis cycle of the composite is typical for ferromagnetic material. The saturation magnetization value of about 6 (emu/g) is sufficient to allow the separation of the composite adsorbent from aqueous solutions by applying an external magnet, as proven by the insert image (Fig. 6).

Results emerged from SEM analysis (Fig.7a–c) revealed the presence of ripples distributed uniformly onto the surface of the composite particle. The ripples induce a type of roughness to the surface that might affect beneficially the adsorption efficiency by increasing the contact area. Likewise, the non-uniform distribution of voids can be distinguished from Fig.7a–c. Such voids (2–10 μm in size) represent macro-pores that can promote the intra-particle diffusion. The EDX spectrum (Fig. 7d) indicates the presence of all the expected chemical elements (C, O, Ca, Ni and Fe).

Infrared spectra of the sodium alginate, calcium alginate and $NiFe_2O_4$@Ca-alginate are compared in Fig.8(a–c). The spectrum of

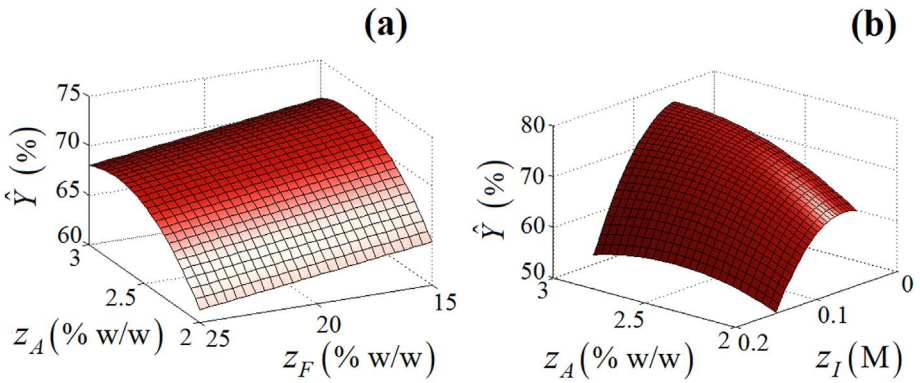

Fig. 4. Response surface plots showing the coupling effects of factors on the color removal efficiency (removal of Rh6G dye): (a) effects of factors z_A and z_F (at z_I = 0.1 M); (b) effects of factors z_A and z_I (at z_F = 20% w/w).

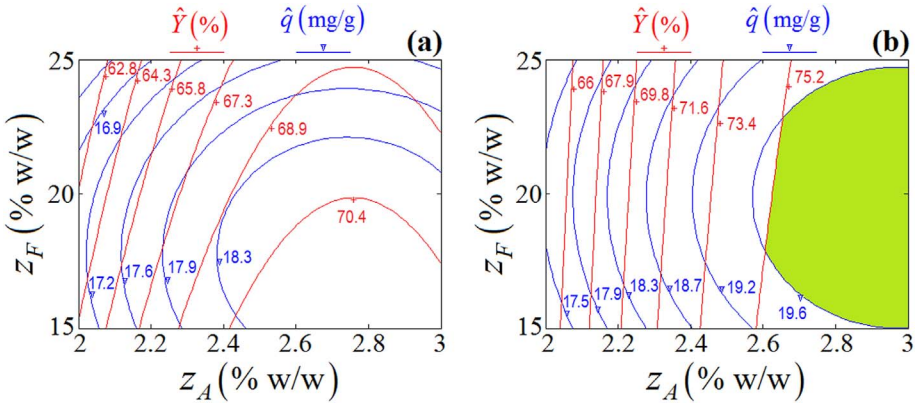

Fig. 5. Overlap contour-lines maps of response functions $\hat{Y}$ and $\hat{q}$ depending on factors $z_A$and z_F: (a) for the constant level of z_I = 0.1 (M); (b) for the constant level of z_I = 0.05 (M).

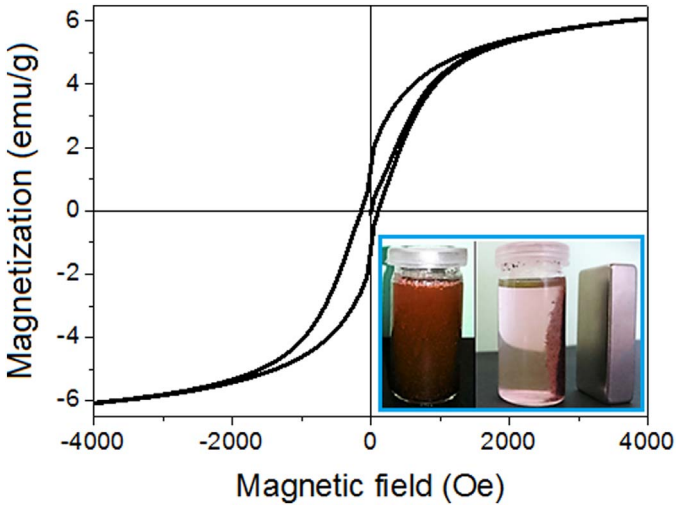

Fig. 6. Plots showing the magnetic properties of the composite adsorbent ($NiFe_2O_4$@Ca-alginate); main image - hysteresis cycle for the composite; inset image – separation of the dye-loaded composite adsorbent under the external magnetic field.

sodium alginate is in good agreement with literature [47]. The main absorption bands were attributed to hydroxyl groups (in the range 3200–3600 cm^{-1}) and carboxylic groups (at 1632 cm^{-1} and 1410 cm^{-1}, for asymmetric and symmetric stretching vibrations, respectively). The absorption band recorded in the range 2930–2840 cm^{-1} accounted for the stretching vibration of aliphatic groups C—H. In turn, bands in the range 1115–1005 cm^{-1} were assigned to C—O stretching vibrations [47,48]. As expected, the spectrum of calcium alginate was very similar to the one of sodium alginate. Nevertheless, the cross-linking slightly shifted the wavenumber of asymmetric stretching vibration of carboxyl peak from 1632 cm^{-1} to 1629 cm^{-1}. This fact is explained in literature by the differences between the ionic radius, charge density and atomic weight of sodium and calcium cations [47]. The presence of the nickel ferrite accounted for the appearance of two bands in the IR spectrum of the composite. Therefore, the absorption bands at 585 cm^{-1} and 398 cm^{-1} were typical for spinel ferrite materials and were attributed to the stretching vibration of the tetrahedral metal–oxygen (M—O) bond and the octahedral M—O bond, respectively [41].

3.5. Effects of pH and sorbent dosage

The effect of initial pH on cationic dyes removal is presented in Fig. 9a. As one can see, the removal efficiency obviously increased with the increment of pH from 3.0 to 6.5 for both cases (i.e. removal of Rh6G and MB). For higher pH values (pH 6.5 to 8.0) the removal efficiency slightly decreased for Rh6G, but remained almost stationary for MB. In summary, the maximum removal efficiency was observed near pH 6.5. Therefore, the next studies were conducted at pH 6.5 ± 0.2.

The effect of *sorbent dosage* (*SD*) on the removal efficiency (*Y*, %) of cationic dyes (Rh6G and MB) were also investigated. All experiments related to the sorbent dosage effect were done in triplicate to test the reproducibility of the method. Therefore, the average values of removal efficiency along with standard deviations (error bars) are reported against the sorbent dosage in Fig. 9b. Note that, the reproducibility errors were < 2%. According to Fig. 9b, the increasing of sorbent dosage above 2 g/L revealed a slight diminishing trend for the removal efficiency.This can be attributed to the fact that for *SD* > 2 g/L, the adsorption equilibrium of cationic dyes was almost attained, and the removal efficiency did not change too much.

In addition, desorption experiments were done in batch mode by mixing (for 1 h) the spent sorbents (loaded with Rh6G or MB) with different types of eluents (15 mL), see *ESI* Fig. S1. Results revealed a maximum release of 58.6% of Rh6G in 0.01 M HCl. In turn, the salt solution (0.5 M NaCl) was the most appropriate liquid to ensure the highest desorption (27.5%) of MB from the spent sorbent.

3.6. Adsorption kinetics

The adsorption of cationic dyes (Rh6G and MB) onto the alginate-based composite (AC20) was investigated as a function of *time* for pH 6.5 ± 0.2 and T = 298 K. Fig. 10 highlights the relationship between adsorption capacity q_t (mg/g) and the contact time t (min). Adsorption kinetics data are reported for the removal of Rh6G (Fig. 10a) and MB (Fig. 10b). Generally, the adsorption capacity increases as the contact time elapse. For our peculiar cases, q_t increased very fast in the first moments (t < 5 min) and then much slower. According to observations (Fig. 10), the uptake of cationic dyes by alginate-based composite (AC20) attained the equilibrium in about 90 min contact time.

Conventional and advanced kinetic models [49–52] were applied to fit experimental data, namely: *a*) pseudo-first order kinetics (PFO); *b*) pseudo-second order kinetics (PSO); *c*) pseudo-n-order kinetics (PnO); *d*) mixed 1,2-order kinetics (MOE) and *e*) intra-particle diffusion kinetics (ID). Mathematical expressions of kinetic models are listed in Table 3 along with the calculated parameters. Herein, q_e (mg/g) denotes the amount of dye adsorbed onto the solid surface at equilibrium for the given conditions. And, q_t (mg/g) is the adsorption capacity at any contact time. Note that, parameters of kinetic models were computed by Gauss-Newton non-linear regression method using built-in solver (*nlinfit*) in the *matlab* program. Predictions provided by kinetic models were plotted as solid, dashed and dot lines in Fig. 10. To assess the overall fit between predictions and observations, the *chi-square test* (χ^2) was employed as the error function [53,54]:

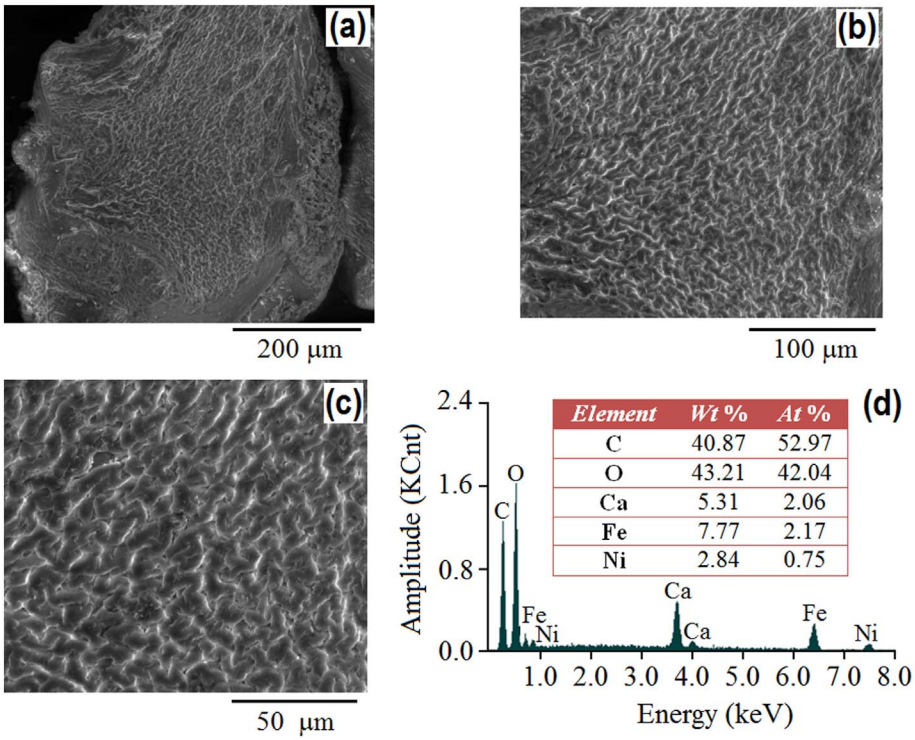

Fig. 7. SEM-EDX analysis and plots of the composite adsorbent AC20 ($NiFe_2O_4$@Ca-alginate): (a, b, c) SEM images of the composite material at different magnitudes; (d) EDX spectrum of the composite material.

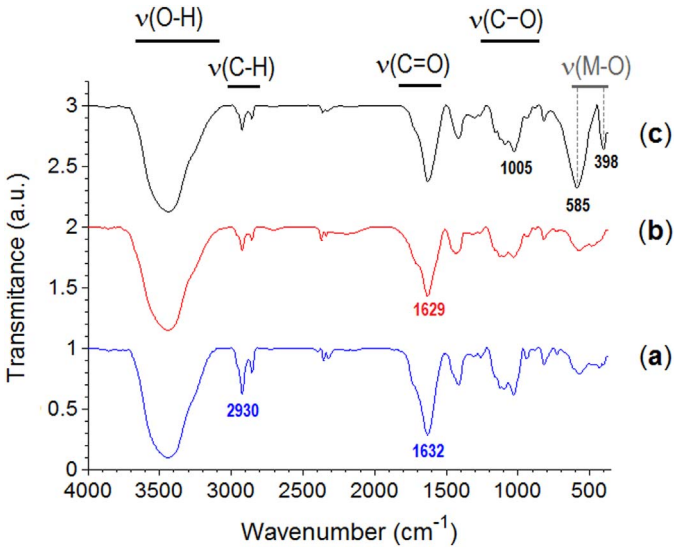

Fig. 8. FTIR absorption spectra of (a) sodium alginate; (b) cross-linked alginate with Ca^{2+} ions; (c) $NiFe_2O_4$@Ca-alginate (AC20).

$$\chi^2 = \sum_i \frac{(q_i^{(calc)} - q_i^{(obs)})^2}{q_i^{(calc)}} \quad (8)$$

where $q^{(obs)}$ is the observed adsorption capacity (mg/g); $q^{(calc)}$ - calculated adsorption capacity (mg/g); and i - integer index of summation indicating the successiveness of the experimental data.

Note that, smaller values of the error function (χ^2) suggest a better prediction ability of the model. As reported in Table 3, the χ^2-values suggested that kinetic models PnO, MOE, PSO and PFO provided well-fitting predictions. By contrast, the intraparticle-diffusion model (ID) emerged as a poorer model for fitting experimental observations. This evidence suggested that the voids from the material surface (Fig. 7a–c), and respectively intra-particle diffusion, might be of secondary importance for influencing the adsorption capacity. According to Fig. 10a, the adsorption of Rh6G onto AC20-sorbent was closer to the *second order kinetics*, because of $n = 2.146$ (PnO) and the smallest χ^2-value associated with PSO model (Table 3). For the case of MB adsorption onto AC20 (Fig. 10b) the system was closer to the *first order kinetics* owing to $n = 1.243$ (PnO), and smaller χ^2-value attributed to PFO model as compared to PSO (Table 3).

3.7. Adsorption isotherms

In this section, the adsorption isotherms for cationic dyes uptake by the alginate-based composite (AC20) were determined at three levels of temperature. The contact time was fixed at $t = 180$ min to attain a complete equilibrium. Fig. 11 reports the isotherm data for the adsorption of Rh6G (Fig. 11a) and MB (Fig. 11b) onto the solid surface of the alginate-based composite (AC20). Herein, the adsorption capacity q_e (mg/g) versus the dye equilibrium concentration C_e (mg/L) is plotted. As shown in Fig. 11, the adsorption capacity gradually increases with the increment of the equilibrium concentration. The increasing trend is slower for the Rh6G/AC20 system (Fig. 11a) comparing to MB/AC20 (Fig. 11b). Experimental observations revealed a remarkable adsorption capacity of AC20 sorbent that was equal to 845 mg/g (for Rh6G uptake) and 1243 mg/g (for MB adsorption). These values of maximal adsorption capacity were observed at the temperature of 298 K (25 °C). Moreover, the attachment of the cationic dye (Rh6G or MB) onto the adsorbent (AC20) was not favored as the temperature increased (Fig. 11).

To bring more details about the adsorption equilibrium, the data were subjected to modeling using isotherm models with three parameters, namely Sips and Redlich-Peterson (R-P). Both models (Sips and R-P) present features of the classical Langmuir and Freundlich isotherm equations [55]. Sips isotherm model is given by:

$$q_e = \frac{q_S\, b\, C_e^{1/n}}{1 + b\, C_e^{1/n}} \quad (9)$$

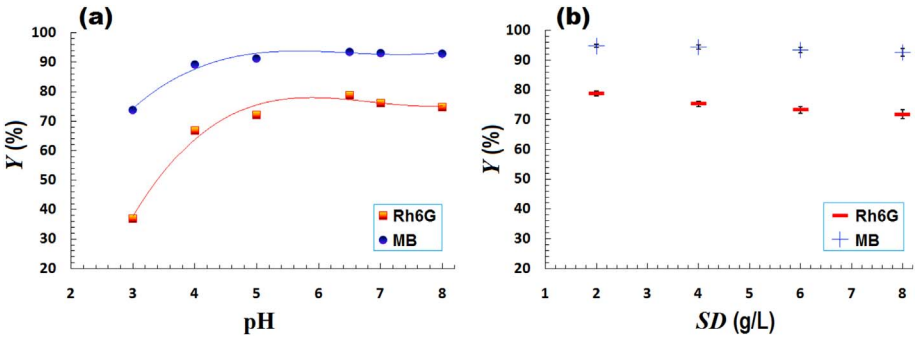

Fig. 9. Effect of pH (a) and sorbent dosage *SD* (b) on color removal efficiency of cationic dyes (Rh6G and MB); C_0 = 50 mg/L; t = 180 min; T = 298 K.

where q_e (mg/g) and C_e (mg/L) are the adsorption capacity and dye concentration at equilibrium, respectively; q_S, b and n are Sips model parameters. Concerning the Redlich-Peterson (R-P) model, this isotherm equation can be described by the next expression:

$$q_e = \frac{A\,C_e}{1 + B\,C_e^g} \tag{10}$$

where A and B are R-P isotherm parameters, whereas g is the R-P isotherm exponent that varies from 0 to 1. A special case emerges when the exponent is equal to unity ($g = 1$), and the R-P model overlays with Langmuir model. The parameters of Sips and R-P isotherm models were calculated by *Gauss-Newton* non-linear regression method. To assess the goodness-of-fit between observations and predictions, the error function (χ^2) was also calculated according to Eq.(8). Tables 4 and 5 summarize the values of isotherms parameters and χ^2 error functions for studied systems Rh6G/AC20 and MB/AC20, respectively.

As detailed in Fig. 11, both isotherm models (Sips and R-P) were appropriate for fitting the equilibrium adsorption data. In all cases, the exponent factor for R-P model converged to unity ($g = 1$) suggesting the overlap of R-P with Langmuir model. Therefore, the R-P isotherm parameter B is identical with the Langmuir isotherm constant (K_L). This special case when R-P model converges to Langmuir isotherm is typical for dyes adsorption systems [56]. To establish the type of adsorption process, the equilibrium data were additionally analyzed by *Dubinin-Radushkevich* (D-R) isotherm model. Details about D-R isotherm are given in Refs [57,58]. Main parameters of D-R isotherm are reported in Tables 4–5, i.e. the constant K_D (mol^2 kJ^{-2}) and the *mean free energy of sorption* E_S (kJ/mol). If the mean free energy is < 8 (kJ/mol), the process is mainly based on the physical adsorption. In turn, if E_S lies between 8 and 16 (kJ/mol), the process can be explained by ion-exchange mechanism [57,58]. In our case, the mean free energy was ranged from 7.23 to 7.84 (kJ/mol) for Rh6G/AC20 system, and between 8.71 and 9.26 (kJ/mol) for MB/AC20. Hence, it turns out that the adsorption mechanism of cationic dyes onto the composite ($NiFe_2O_4$@Ca-alginate) is based on both, physical interactions and ion exchange. In particular, physical interactions were predominant for Rh6G/AC20, whereas the ion-exchange was principal for the MB/AC20 system.

3.8. Thermodynamic parameters

Thermodynamic parameters for the adsorption of Rh6G and MB dyes onto $NiFe_2O_4$@Ca-alginate (AC20 sample) were calculated according to the methodology presented in detail elsewhere [2,55]. The results of thermodynamics analysis are summarized in Table S4 (*ESI*). This table reports the values of *Gibbs* free energy (ΔG), enthalpy (ΔH) and entropy (ΔS) of the adsorption process. The negative values of *Gibbs* free energy (ΔG, −15.04 and −19.61 kJ/mol) indicated the spontaneous nature of investigated adsorption processes. The resulted values of enthalpy suggested a moderate endothermic effect for the Rh6G/AC20 system (ΔH = 4.53 kJ/mol) and an exothermic effect for the adsorption of MB onto AC20 (ΔH = −24.12 kJ/mol). The change in entropy values was positive for Rh6G/AC20 and negative for MB/AC20 (see *ESI,* Table S4) suggesting the increase/decrease of the randomness at the adsorbent-liquid interface, respectively.

Table 6 compares the adsorption performance of the composite ($NiFe_2O_4$@Ca-alginate) and other sorption materials reported in the literature. As given in Table 6, our composite revealed a high sorption capacity comparing to materials listed in the table.

3.9. Molecular docking simulations

Molecular docking is a computational chemistry tool applied for predicting noncovalent binding and affinity between a macromolecule (receptor) and a small molecule (ligand), starting from their unbound structures [62]. In this study, for molecular docking simulations we used the AutoDock-Vina method [62] implemented in the YASARA Structure software package.

It is well known that alginate is a linear copolymer with homopolymeric blocks of (1–4)-linked β-D-mannuronate (M) and its α-L-guluronate (G) monomeric units (residues). These M and G-residues are

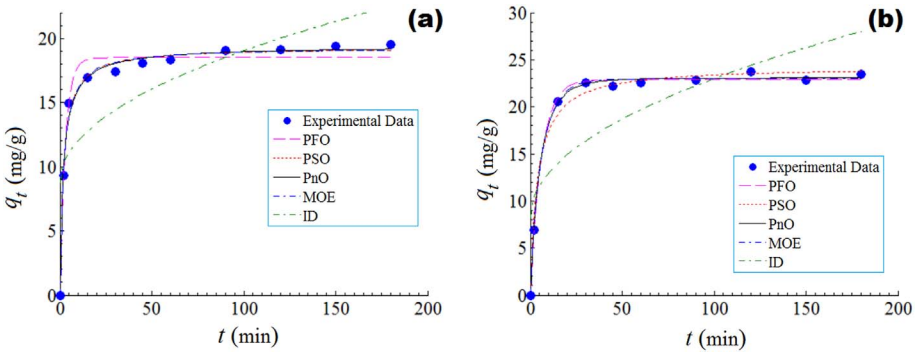

Fig. 10. Adsorption kinetics of cationic dyes onto $NiFe_2O_4$@Alginate-Ca composite adsorbent (sample: AC20) and the comparison of different fitted models; (a) Adsorption kinetics data for Rh6G uptake; (b) Adsorption kinetics data for MB uptake; T = 298 K, *SD* = 2 g/L, C_o = 50 mg/L and pH 6.5 ± 0.2.

Table 3
Kinetic models and parameters for cationic dyes adsorption (Rh6G and MB) onto the optimal composite adsorbent AC20 ($NiFe_2O_4$@Ca-alginate).

Abbreviation	Kinetic model (non-linear equation)	Kinetic parameters (Rh6G/AC20)	Kinetic parameters (MB/AC20)
PFO[a]	$q_t = q_e(1 - e^{-k_1 t})$	q_e = 18.491 (mg/g) k_1 = 0.3358 χ^2 = 0.3347	q_e = 22.868 k_1 = 0.1667 χ^2 = 0.1044
PSO[b]	$q_t = \frac{k_2 q_e^2 t}{1 + k_2 q_e t}$	q_e = 19.276 (mg/g) k_2 = 0.0269 χ^2 = 0.16794	q_e = 24.291 k_2 = 0.0104 χ^2 = 0.3933
PnO[c]	$q_t = q_e - [(n-1)k_n t + q_e^{(1-n)}]^{\frac{1}{1-n}}$	q_e = 19.466 (mg/g) $k_n = 1.8317 \times 10^{-2}$ n = 2.146 χ^2 = 0.17355	q_e = 23.050 $k_n = 8.8019 \times 10^{-2}$ n = 1.243 χ^2 = 0.0583
MOE[d]	$q_t = q_e \frac{1 - e^{(-K_1 t)}}{1 - \frac{K_2 q_e}{K_1 + K_2 q_e} e^{(-K_1 t)}}$	q_e = 19.276 (mg/g) $K_1 = 1.4404 \times 10^{-6}$ $K_2 = 2.6943 \times 10^{-2}$ χ^2 = 0.16805	q_e = 22.958 $K_1 = 1.2277 \times 10^{-1}$ $K_2 = 2.942 \times 10^{-3}$ χ^2 = 0.0654
ID[e]	$q_t = k_d \sqrt{t} + J$	k_d = 1.0225 J = 8.7975 χ^2 = 4.564	k_d = 1.4694 J = 8.2835 χ^2 = 9.2105

[a] PFO - pseudo-first order kinetics.
[b] PSO - pseudo-second order kinetics.
[c] PnO - pseudo-n-order kinetics.
[d] MOE - mixed 1,2-order kinetics.
[e] ID - intra-particle diffusion kinetics.

covalently linked together in different sequences or blocks. To simulate a short alginate oligomer chain we used both mannuronate (M) and guluronate (G) monomer units (residues) downloaded from the CarbBuilder data-base [63]. Afterwards, by using YASARA program we build two alginate linear-chains (oligomers: A1 and A2), each one consisting of eight residues (i.e. MMGGMMGG-block). Hence, each oligomer chain (A1 and A2) contained eight carboxylic groups ($-COO^-$) carrying a total charge of (−8). To simulate crosslinking points between alginate chains A1 and A2 (aligned in parallel and symmetrically) we added four calcium ions ($4 \times Ca^{2+}$) along and between oligomer chains.

Molecular structures of cationic dyes (Rh6G and MB, each one carrying a net charge +1) were built in YASARA program and optimized first at the level of PM3 semi-empirical molecular orbital theory. Speaking in the terminology of molecular docking, the cationic dyes play the role of the *ligands*. In turn, the calcium-alginate supramolecular structure (A1-Ca-A2) has the role of the *receptor* in molecular docking simulations. Subsequently, all structures (*ligands* and *receptor*) were subjected to energy minimization at the level of self-parameterizing knowledge-based YASARA force field [64].During molecular docking simulations, the *receptor* (A1-Ca-A2) was treated as a rigid structure, whereas *ligands* (Rh6G and MB) were treated as flexible molecules.

The molecular computations (by AutoDock-VINA method) were performed using a number of 100 docking runs followed by the cluster analysis. For each complex conformation, the *free binding energy* (E_b, kcal/mol) was computed to reproduce chemical potentials in accordance with AutoDock-VINA method.

Fig. 12 shows the results of molecular docking simulation describing the interaction between calcium-alginate (*receptor*: A1-Ca-A2) and Rh6G dye (*ligand*). According to this figure, calcium ions were re-positioned (after energy minimization) into the "pockets" formed between alginate chains (A1 and A2) and by attracting adjacent carboxylic groups from both sides. These pockets represent in fact the cross-linking points between alginate linear chains. Likewise, the molecular modeling results unveiled the formation of hydrogen-bonds (H-bonds) between alginates residues (M/G), i.e. between hydroxyl (−OH), carboxyl ($-COO^-$) and glycosidic (−O−) groups (Fig. 12). According to AutoDock-VINA method, the free energy of binding between calcium-alginate and Rh6G dye was equal to $E_b = -5.89$ kcal/mol, being attributed for the best docked-complex conformation. In this case, the Rh6G molecule was interacted with 10 alginate residues from both chains A1 and A2, summing up a total number of 204 interatomic contacts (considering a cut-off radius < 4 Å). From these, 83 interatomic contacts were attributed for the interaction of Rh6G with *four* G-residues, and 121 contacts as a result of interaction with *six* M-residues. In addition, the docking results and clustering analysis revealed the possibility of hydrogen-bond formation between a hydroxyl group (proton donor) from alginate and carbonyl group (proton acceptor) from Rh6G molecule.

The interaction (molecular docking outcome) between calcium-

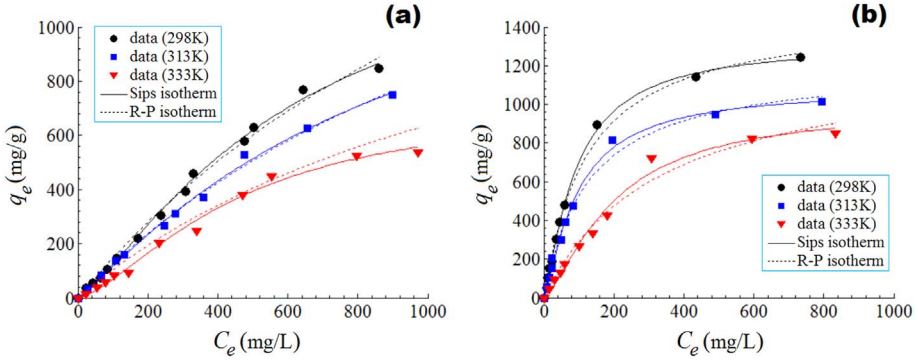

Fig. 11. Equilibrium adsorption (isotherms) of cationic dyes onto $NiFe_2O_4$@Alginate-Ca composite adsorbent (sample: AC20) and the comparison of different fitted models; (a) Adsorption isotherms data for Rh6G uptake; (b) Adsorption isotherms data for MB uptake;t = 180 min, SD = 2 g/L, pH 6.5 ± 0.2.

Table 4
Isotherm parameters for Rh6G dye adsorption onto the optimal composite adsorbent AC20 ($NiFe_2O_4$@Alginate-Ca).

Isotherm	Adsorbent composite AC20 (Alginate/$NiFe_2O_4$)		
	T = 298 K (25 °C)	T = 313 K (40 °C)	T = 333 K (60 °C)
Redlich-Peterson	A = 1.5635	A = 1.3354	A = 1.0109
A	$B = 6.0157 \times 10^{-4}$	$B = 6.3795 \times 10^{-4}$	$B = 7.2794 \times 10^{-4}$
B	g = 1	g = 1	g = 1
g	χ^2 = 23.378	χ^2 = 6.7093	χ^2 = 63.324
Sips	q_S = 1420.0	q_S = 1527.5	q_S = 733.2
q_S (mg/g)	$b = 2.3873 \times 10^{-4}$	$b = 4.5473 \times 10^{-4}$	$b = 9.1772 \times 10^{-5}$
b	n_S = 0.76909	n_S = 0.88587	n_S = 0.65842
n	χ^2 = 22.312	χ^2 = 7.8616	χ^2 = 26.307
Dubinin-Radushkevich			
K_D ($mol^2\,kJ^{-2}$)	$K_D = 9.5613 \times 10^{-3}$	$K_D = 8.31162 \times 10^{-3}$	$K_D = 8.12321 \times 10^{-3}$
E_S (kJ/mol)	E_S = 7.23	E_S = 7.75	E_S = 7.84

alginate (*receptor*: A1-Ca-A2) and MB dye (*ligand*) is depicted in Fig. 13. In this instance, the free energy of binding was found to be $E_b = -5.46$ kcal/mol accounting for the interaction of MB with seven alginate residues (3 × M and 4 × G). The total number of interatomic contacts between alginate and MB molecule was equal to 155 (i.e., 51 contacts with M units and 104 contacts with G residues).

It should be mentioned that the free energy of binding (E_b) computed by the AutoDock-VINA algorithm was employed to approximate the chemical potentials of the system and to perform docking and virtual screening simulations. The calculation of this energy (E_b) in docking program is mainly based on scoring function and this approach is seen as more like to "machine learning" [62]. Therefore, we considered proper to calculate additionally and the *interaction energy* (ΔE) between the *ligand* and *receptor* on the basis of molecular force field that can be expressed as follows:

$$\Delta E = E_D - (E_R + E_L) \quad (11)$$

where, ΔE denotes the energy of interaction between *ligand* and *receptor*, E_D is the energy of the docked complex; E_R – energy of the *receptor*, and E_L – energy of the *ligand*. Note that all energy terms listed in Eq.(11) were referred to the potential energy computed on the basis of YASARA molecular mechanics force field. And, each term included both *intramolecular* and *intermolecular* parts. The latter one comprised two individual energy components such as *Van-der-Waals* (VdW) and *Coulomb* that were responsible for distance-dependent attractive/repulsive interactions and electrostatic effects, respectively. Normally, the lower the energy, the stronger is the interaction between molecular entities.

Table 7 summarizes the energies of intermolecular interactions between cationic dyes (*ligands*) and calcium alginate (*receptor*: A1-Ca-A2). As detailed in Table 7, the interaction between Rh6G and alginate mostly relied on *V*dW forces ($\Delta E_{VdW} = -25.93$ kcal/mol), whereas the electrostatic interactions ($\Delta E_{CL} = -11.46$ kcal/mol) were of secondary importance. By contrast, for the case of alginate binding with MB, the primary role was attributed to electrostatic interactions ($\Delta E_{CL} = -32.65$ kcal/mol), while the VdW forces

Table 6
Comparison of adsorption capacity of different sorbent materials for uptake of cationic dyes.

Adsorbent	Dye	Adsorption capacity [mg/g]	Ref.
Chitosan clay nanocomposite	Rhodamine 6G	441	[2]
Montmorillonite–Alginate	Basic red 46 (BR46)	35	[3]
Carboxylic acid modified resin	Methylene blue	300	[11]
Dried twigs of *Melaleuca diosmifolia*	Methylene blue	119	[15]
Rice Husk Ash (RHA)	Methylene blue	18	[17]
Calcium alginate beads	Basic black dye	58	[27]
Alginate–clay quasi-cryogel beads	Methylene Blue	182	[34]
Alginate/TiO_2	Direct Red 80	164	[35]
Graphene/alginate nanocomposite	Methylene blue	850	[36]
Graphene oxide/Ca-alginate	Methylene blue	182	[37]
Nickle-zinc ferrite-alginate composite	Basic blue 9	106	[38]
Activated carbon powder into calcium-alginate beads	Methylene blue	986	[59]
Bentonite – alginate composite	Crystal violet	601	[60]
Sodium alginate/Na + -rectorite composite microspheres	Basic blue	493	[61]
$NiFe_2O_4$@Ca-alginate	Rhodamine 6G	845	This study
$NiFe_2O_4$@Ca-alginate	Methylene blue	1243	This study

Table 5
Isotherm parameters for MB dye adsorption onto the optimal composite adsorbent AC20 ($NiFe_2O_4$@Alginate-Ca).

Isotherm	Adsorbent composite AC20 (Alginate/$NiFe_2O_4$)		
	T = 298 K (25 °C)	T = 313 K (40 °C)	T = 333 K (60 °C)
Redlich-Peterson	A = 11.9910	A = 9.4152	A = 3.7789
A	$B = 8.1249 \times 10^{-3}$	$B = 7.7954 \times 10^{-3}$	$B = 2.9922 \times 10^{-3}$
B	g = 1	g = 1	g = 1
g	χ^2 = 36.446	χ^2 = 33.584	χ^2 = 40.686
Sips	q_S = 1325.4	q_S = 1085.0	q_S = 991.8
q_S (mg/g)	$b = 3.6331 \times 10^{-3}$	$b = 3.1089 \times 10^{-3}$	$b = 5.7000 \times 10^{-4}$
b	n_S = 0.80226	n_S = 0.79043	n_S = 0.70751
n	χ^2 = 16.719	χ^2 = 18.275	χ^2 = 49.798
Dubinin-Radushkevich			
K_D ($mol^2\,kJ^{-2}$)	$K_D = 6.58893 \times 10^{-3}$	$K_D = 5.82643 \times 10^{-3}$	$K_D = 6.26369 \times 10^{-3}$
E_S (kJ/mol)	E_S = 8.71	E_S = 9.26	E_S = 8.93

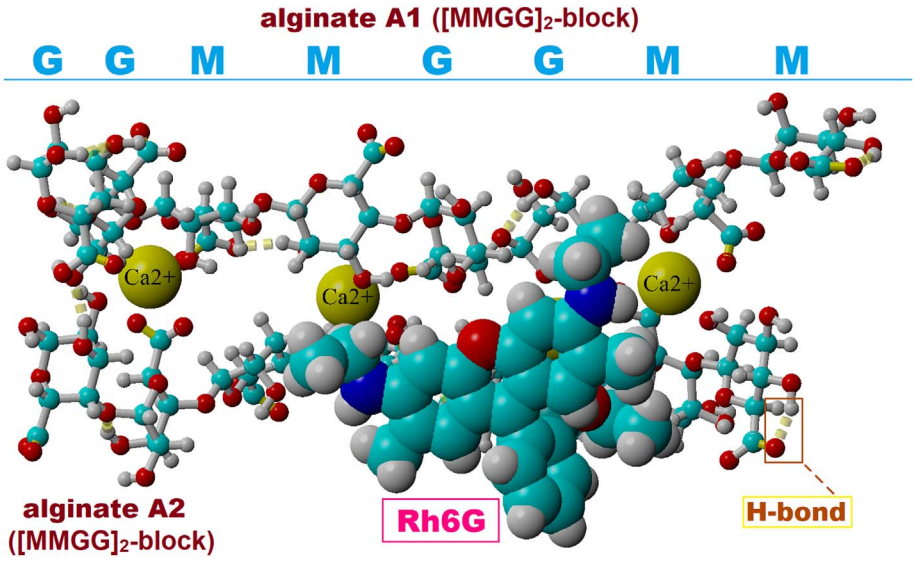

Fig. 12. Molecular docking simulation results detailing the interactions between Rhodamine 6G molecule (Rh6G) and alginate oligomers (MMGGMMGG-blocks) cross-linked with Ca^{2+} ions.

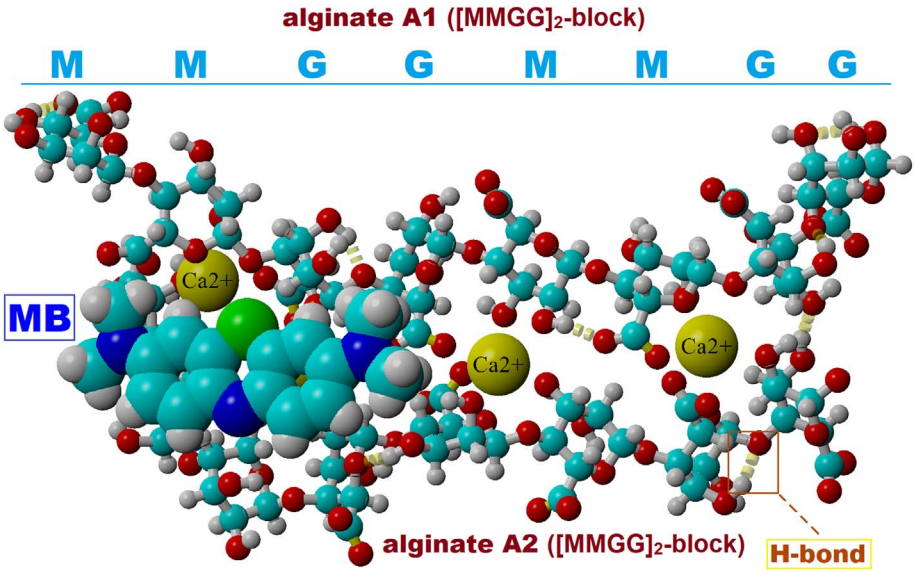

Fig. 13. Molecular docking simulation results detailing the interactions between Methylene Blue molecule (MB) and alginate oligomers (MMGGMMGG-blocks) cross-linked with Ca^{2+} ions.

Table 7
Energy of intermolecular interactions between cationic dyes (ligands) and calcium alginate (receptor: A1-Ca-A2) calculated for the docked complexes.

Docking system (ligand/ receptor)	*Total intermolecular:* $\Delta E = \Delta E_{VdW} + \Delta E_{CL}$, (kcal/mol)	*Van-der-Waals:* ΔE_{VdW}, (kcal/mol)	*Coulomb:* ΔE_{CL}, (kcal/mol)
Rh6G/Ca-alginate	−37.39	−25.93	−11.46
MB/Ca-alginate	−54.71	−22.06	−32.65

($\Delta E_{VdW} = -22.06$ kcal/mol) were of subsidiary significance. The different interaction behavior of dyes with alginate might be connected to molecular surfaces. For instance, the molecular surface of Rh6G and MB is equal to 413 $Å^2$ and 274 $Å^2$, respectively. Hence, the Rh6G and MB dyes carry the same charge, but associated to the different molecular surfaces. It may seem that the greater molecular surface, the more important is VdW interaction.

Overall, the total intermolecular interaction energy ($\Delta E = \Delta E_{VdW} + \Delta E_{CL}$) was lower for the MB/alginate system (Table 7), suggesting that calcium-alginate interacted better with MB compared to Rh6G. These simulation findings are in reasonable agreement with D-R isotherm results. Hence, the adsorption mechanism of cationic dyes onto calcium alginate is based on both physical adsorption and ion exchange, but the contribution of these phenomena depends on the chemical structure and molecular surface of each molecule.

4. Conclusions

In summary, we demonstrated a method to produce $NiFe_2O_4$@Ca-alginate composite adsorbent as plate-like micro-particles able to be magnetically separable after usage. Composite materials were formulated in accordance with a second-order design of experiments and response surface methodology. The optimal formulation of $NiFe_2O_4$@Ca-alginate composite involved a content of 16% (*w*/w) $NiFe_2O_4$ nanoparticles into the composite matrix. In addition, this

material was characterized by SEM, EDAX, FTIR and magnetic measurements.

The dynamics of adsorption processes were well-fitted by kinetic models (PFO, PSO, PnO and MOE). Sips and Redlich-Peterson isotherm models revealed good agreements with the experimental equilibrium data. The maximal adsorption capacity was observed at the temperature of 298 K and it was equal to 845 mg/g (for Rh6G adsorption) and 1243 mg/g (for MB uptake). According to Dubinin-Radushkevich isotherms, the mean free energy values of adsorption *Es* ranged from 7.23 to 9.26 (kJ/mol) suggesting the contribution of both physical and ion-exchange interactions. The thermodynamic analysis indicated that the investigated adsorption processes occurred spontaneously owing to the negative values of *Gibbs* free energy ($\Delta G \leq -15$ kJ/mol).

To gain more insights about interactions between cationic dyes and calcium alginate (MMGGMMGG-block), we performed the molecular docking simulations using AutoDock-Vina method and YASARA-Structure program. Simulation outcomes revealed that the binding mechanism between cationic dyes and alginate involved both *Van-der-Waals* and electrostatic (*Coulomb*) intermolecular interactions.

Acknowledgment

This work was supported by a grant of the Romanian National Authority for Scientific Research and Innovation, CNCS – UEFISCDI, grant agreement No 95/01.10.2015, project number PN-II-RU-TE-2014-4-1266. The research related to molecular docking simulations is a part of a project that has received funding from the European Union's Horizon 2020 research and innovation program under the grant agreement No 667387 WIDESPREAD 2-2014 SupraChem Lab.

Appendix A. Supplementary data

Supplementary data to this article can be found online at https://doi.org/10.1016/j.reactfunctpolym.2018.02.008.

References

[1] M.T. Yagub, T.K. Sen, S. Afroze, H.M. Ang, Dye and its removal from aqueous solution by adsorption: a review, Adv. Colloid Interf. Sci. 209 (2014) 172–184, http://dx.doi.org/10.1016/j.cis.2014.04.002.

[2] A. Vanamudan, P. Pamidimukkala, Chitosan, nanoclay and chitosan–nanoclay composite as adsorbents for Rhodamine-6G and the resulting optical properties, Int. J. Biol. Macromol. 74 (2015) 127–135, http://dx.doi.org/10.1016/j.ijbiomac.2014.11.009.

[3] A. Hassani, R.D. Cheshmeh Soltani, S. Karaca, A. Khataee, Preparation of montmorillonite–alginate nanobiocomposite for adsorption of a textile dye in aqueous phase: isotherm, kinetic and experimental design approaches, J. Ind. Eng. Chem. 21 (2015) 1197–1207, http://dx.doi.org/10.1016/j.jiec.2014.05.034.

[4] K.B. Tan, M. Vakili, B.A. Horri, P.E. Poh, A.Z. Abdullah, B. Salamatinia, Adsorption of dyes by nanomaterials: recent developments and adsorption mechanisms, Sep. Purif. Technol. 150 (2015) 229–242, http://dx.doi.org/10.1016/j.seppur.2015.07.009.

[5] A. Garg, M. Mainrai, V. Kumar Bulasara, S. Barman, Experimental investigation on adsorption of Amido Black 10B dye onto zeolite synthesized from fly ash, Chem. Eng. Commun. 202 (2015) 123–130, http://dx.doi.org/10.1080/00986445.2013.836636.

[6] Y. Gao, S. Xu, Q. Yue, Y. Wu, B. Gao, Chemical preparation of crab shell-based activated carbon with superior adsorption performance for dye removal from wastewater, J. Taiwan Inst. Chem. Eng. 61 (2016) 327–335, http://dx.doi.org/10.1016/j.jtice.2015.12.023.

[7] E. Kacan, B.E.T. Optimum, surface areas for activated carbon produced from textile sewage sludges and its application as dye removal, J. Environ. Manag. 166 (2016) 116–123, http://dx.doi.org/10.1016/j.jenvman.2015.09.044.

[8] Q.H. Hu, S.Z. Qiao, F. Haghseresht, M.A. Wilson, G.Q. Lu, Adsorption Study for Removal of Basic Red Dye Using Bentonite, Ind. Eng. Chem. Res. 45 (2006) 733–738, http://dx.doi.org/10.1021/ie050889y.

[9] D. Karadag, E. Akgul, S. Tok, F. Erturk, M.A. Kaya, M. Turan, Basic and Reactive Dye Removal Using Natural and Modified Zeolites, J. Chem. Eng. Data 52 (2007) 2436–2441, http://dx.doi.org/10.1021/je7003726.

[10] M. Wawrzkiewicz, Anion-exchange resins for C.I. direct blue 71 removal from aqueous solutions and wastewaters: effects of basicity and matrix composition and structure, Ind. Eng. Chem. Res. 53 (2014) 11838–11849, http://dx.doi.org/10.1021/ie501992n.

[11] E. Yavuz, G. Bayramoğlu, M.Y. Arica, B.F. Senkal, Preparation of poly (acrylic acid) containing core-shell type resin for removal of basic dyes, J. Chem. Technol. Biotechnol. 86 (2011) 699–705, http://dx.doi.org/10.1002/jctb.2571.

[12] M. Wawrzkiewicz, Z. Hubicki, Kinetics of adsorption of sulphonated azo dyes on strong basic anion exchangers, Environ. Technol. 30 (2009) 1059–1071, http://dx.doi.org/10.1080/09593330903055650.

[13] E.H. Ezechi, S.R. Mohamed Kutty, A. Malakahmad, M. Hasnain Isa, Characterization and optimization of effluent dye removal using a new low cost adsorbent: equilibrium, kinetics and thermodynamic study, Process. Saf. Environ. Prot. 98 (2015) 16–32, http://dx.doi.org/10.1016/j.psep.2015.06.006.

[14] S.Y. Kazemi, P. Biparva, E. Ashtiani, Cerastoderma lamarcki shell as a natural, low cost and new adsorbent to removal of dye pollutant from aqueous solutions: equilibrium and kinetic studies, Ecol. Eng. 88 (2016) 82–89, http://dx.doi.org/10.1016/j.ecoleng.2015.12.020.

[15] S. Kuppusamy, P. Thavamani, M. Megharaj, K. Venkateswarlu, Y. Bok Lee, R. Naidu, Potential of Melaleuca diosmifolia as a novel, non-conventional and low-cost coagulating adsorbent for removing both cationic and anionic dyes, J. Ind. Eng. Chem. 37 (2016) 198–207, http://dx.doi.org/10.1016/j.jiec.2016.03.021.

[16] A. Ebrahimi, M. Arami, H. Bahrami, E. Pajootan, Fish bone as a low-cost adsorbent for dye removal from wastewater: response surface methodology and classical method, Environ. Model. Assess. 18 (2013) 661–670, http://dx.doi.org/10.1007/s10666-013-9369-z.

[17] A.K. Chowdhury, A.D. Sarkar, A. Bandyopadhyay, Rice Husk Ash as a Low Cost Adsorbent for the Removal of Methylene Blue and Congo Red in Aqueous Phases, CleanRooms 37 (2009) 581–591, http://dx.doi.org/10.1002/clen.200900051.

[18] P.S. Kumar, M. Palaniyappan, M. Priyadharshini, A.M. Vignesh, A. Thanjiappan, P.S.A. Fernando, R.T. Ahmed, R. Srinath, Adsorption of basic dye onto raw and surface-modified agricultural waste, Environ. Prog. Sustain. Energy 33 (2014) 87–98, http://dx.doi.org/10.1002/ep.11756.

[19] S. Kahraman, P. Yalcin, H. Kahraman, The evaluation of low-cost biosorbents for removal of an azo dye from aqueous solution, Water Environ. J. 26 (2012) 399–404, http://dx.doi.org/10.1111/j.1747-6593.2011.00300.x.

[20] A.R. Vasques, S.M. Guelli, U. de Souza, J.A.B. Valle, A.A. Ulson de Souza, Application of ecological adsorbent in the removal of reactive dyes from textile effluents, J. Chem. Technol. Biotechnol. 84 (2009) 1146–1155, http://dx.doi.org/10.1002/jctb.2147.

[21] M.M. Abd El-Latif, A.M. Ibrahim, Adsorption, kinetic and equilibrium studies on removal of basic dye from aqueous solutions using hydrolyzed oak sawdust, Desalination Water Treat. 6 (2009) 252–268, http://dx.doi.org/10.5004/dwt.2009.501.

[22] M. Saeed, R. Nadeem, M. Yousaf, Removal of industrial pollutant (Reactive Orange 122 dye) using environment-friendly sorbent Trapa bispinosa's peel and fruit, Int. J. Environ. Sci. Technol. 12 (2015) 1223–1234, http://dx.doi.org/10.1007/s13762-013-0492-9.

[23] M. Vakili, M. Rafatullah, B. Salamatinia, A.Z. Abdullah, M.H. Ibrahim, K.B. Tan, Z. Gholami, P. Amouzgar, Application of chitosan and its derivatives as adsorbents for dye removal from water and wastewater: a review, Carbohydr. Polym. 113 (2014) 115–130, http://dx.doi.org/10.1016/j.carbpol.2014.07.007.

[24] S. Zhao, F. Zhou, L. Li, M. Cao, D. Zuo, H. Liu, Removal of anionic dyes from aqueous solutions by adsorption of chitosan-based semi-IPN hydrogel composites, Composites Part B 43 (2012) 1570–1578, http://dx.doi.org/10.1016/j.compositesb.2012.01.015.

[25] G.L. Dotto, L.A.A. Pinto, Adsorption of food dyes acid blue 9 and food yellow 3 onto chitosan: stirring rate effect in kinetics and mechanism, J. Hazard. Mater. 187 (2011) 164–170, http://dx.doi.org/10.1016/j.jhazmat.2011.01.016.

[26] W. Tan, Y. Zhang, Y. Szeto, L. Liao, A novel method to prepare chitosan/montmorillonite nanocomposites in the presence of hydroxy-aluminum oligomeric cations, Compos. Sci. Technol. 68 (2008) 2917–2921, http://dx.doi.org/10.1016/j.compscitech.2007.10.007.

[27] R. Aravindhan, N.N. Fathima, J.R. Rao, Balachandran Unni Nair, Equilibrium and thermodynamic studies on the removal of basic black dye using calcium alginate beads, Colloids Surf. A Physicochem. Eng. Asp. 299 (2007) 232–238, http://dx.doi.org/10.1016/j.colsurfa.2006.11.045.

[28] T. Lu, T. Xiang, X.L. Huang, C. Li, W.F. Zhao, Q. Zhang, C.S. Zhao, Post-crosslinking towards stimuli-responsive sodium alginate beads for the removal of dye and heavy metals, Carbohydr. Polym. 133 (2015) 587–595, http://dx.doi.org/10.1016/j.carbpol.2015.07.048.

[29] P. Geetha, M.S. Latha, M. Koshy, Biosorption of malachite green dye from aqueous solution by calcium alginate nanoparticles: equilibrium study, J. Mol. Liq. 212 (2015) 723–730, http://dx.doi.org/10.1016/j.molliq.2015.10.035.

[30] F.S. Arakawa, C.R.A. Mahl, S.P.D. Oliveira, G. Igreja, M.R. Simoes, C.F. Silva, Clarification of aqueous Stevia extract using alginate beads – Evaluation by factorial design methodology, Adsorption, Sci. Technol. 30 (2012) 147–158, http://dx.doi.org/10.1260/0263-6174.30.2.147.

[31] S. Uzasci, F. Tezcan, F.B. Erim, Removal of hexavalent chromium from aqueous solution by barium ion cross-linked alginate beads, Int. J. Environ. Sci. Technol. 11 (2014) 1861–1868, http://dx.doi.org/10.1007/s13762-013-0377-y.

[32] X. Vecino, R. Devesa-Rey, J.M. Cruz, A.B. Moldes, Study of the physical properties of calcium alginate hydrogel beads containing vineyard pruning waste for dye removal, Carbohydr. Polym. 115 (2015) 129–138, http://dx.doi.org/10.1016/j.carbpol.2014.08.088.

[33] X. Vecino, R. Devesa-Rey, S. Villagrasa, J.M. Cruz, A.B. Moldes, Kinetic and morphology study of alginate-vineyard pruning waste biocomposite vs. non modified vineyard pruning waste for dye removal, J. Environ. Sci. 38 (2015) 158–167, http://dx.doi.org/10.1016/j.jes.2015.05.032.

[34] G. Uyar, H. Kaygusuz, F. Bedia Erim, Methylene blue removal by alginate–clay quasi-cryogel beads, React. Funct. Polym. 106 (2016) 1–7, http://dx.doi.org/10.

1016/j.reactfunctpolym.2016.07.001.
[35] N.M. Mahmoodi, B. Hayati, M. Arami, H. Bahrami, Preparation, characterization and dye adsorption properties of biocompatible composite (alginate/titania nanoparticle), Desalination 275 (2011) 93–101, http://dx.doi.org/10.1016/j.desal.2011.02.034.
[36] Y. Zhuang, F. Yu, J. Chen, J. Ma, Batch and column adsorption of methylene blue by graphene/alginate nanocomposite: comparison of single-network and double-network hydrogels, J. Environ. Chem. Eng. 4 (2016) 147–156, http://dx.doi.org/10.1016/j.jece.2015.11.014.
[37] Y. Li, Q. Du, T. Liu, J. Sun, Y. Wang, S. Wu, Z. Wang, Y. Xia, L. Xia, Methylene blue adsorption on graphene oxide/calcium alginate composites, Carbohydr. Polym. 95 (2013) 501–507, http://dx.doi.org/10.1016/j.carbpol.2013.01.094.
[38] N.M. Mahmoodi, Magnetic ferrite nanoparticle–alginate composite: synthesis, characterization and binary system dye removal, J. Taiwan Inst. Chem. Eng. 44 (2013) 322–330, http://dx.doi.org/10.1016/j.jtice.2012.11.014.
[39] V. Rocher, A. Bee, J.-M. Siaugue, V. Cabuil, Dye removal from aqueous solution by magnetic alginate beads crosslinked with epichlorohydrin, J. Hazard. Mater. 178 (2010) 434–439, http://dx.doi.org/10.1016/j.jhazmat.2010.01.100.
[40] A. Raschitor, C.M. Fernandez, I. Cretescu, M.A. Rodrigo, P. Canizares, Sono-electrocoagulation of wastewater polluted with Rhodamine 6G, Sep. Purif. Technol. 135 (2014) 110–116, http://dx.doi.org/10.1016/j.seppur.2014.08.003.
[41] P. Samoila, C. Cojocaru, I. Cretescu, C.D. Stan, V. Nica, L. Sacarescu, V. Harabagiu, Nanosized spinel ferrites synthesized by sol-gel autocombustion for optimized removal of azo dye from aqueous solution, J. Nanomater. 2015 (2015), http://dx.doi.org/10.1155/2015/713802 (Article ID 713802, 13 pages), https://www.hindawi.com/journals/jnm/2015/713802/.
[42] D.C. Montgomery, Design and Analysis of Experiments, fifth ed., John Wiley & Sons, New York, 2001.
[43] S. Akhnazarova, V. Kafarov, Experiment Optimization in Che mistry and Chemical Engineering, second ed., Mir Publisher, Moscow, 1982.
[44] M.A. Bezerra, R.E. Santelli, E.P. Oliveira, L.S. Villar, L.A. Escaleira, Response surface methodology (RSM) as a tool for optimization in analytical chemistry, Talanta 76 (2008) 965–977, http://dx.doi.org/10.1016/j.talanta.2008.05.019.
[45] N.R. Costa, J. Lourenco, Z.L. Pereira, Desirability function approach: a review performance evaluation in adverse conditions, Chemom. Intell. Lab. Syst. 107 (2011) 234–244, http://dx.doi.org/10.1016/j.chemolab.2011.04.004.
[46] S.S. Rao, Engineering Optimization Theory and Practice, 4th ed., John Wiley and Sons, New Jersey, 2009.
[47] H. Daemi, M. Barikani, Synthesis and characterization of calcium alginate nanoparticles, sodium homopolymannuronate salt and its calcium nanoparticles, Sci. Iran. 19 (2012) 2023–2028, http://dx.doi.org/10.1016/j.scient.2012.10.005.
[48] C.G. van Hoogmoed, H.J. Busscher, P. de Vos, Fourier transform infrared spectroscopy studies of alginate–PLL capsules with varying compositions, J. Biomed. Mater. Res. 67A (2003) 172–178, http://dx.doi.org/10.1002/jbm.a.10086.
[49] Y.S. Ho, G. McKay, Pseudo-second order model for sorption processes, Process Biochem. 34 (1999) 451–465, http://dx.doi.org/10.1016/S0032-9592(98)00112-5.
[50] R.N. Fallah, S. Azizian, Removal of thiophenic compounds from liquid fuel by different modified activated carbon cloths, Fuel Process. Technol. 93 (2012) 45–52, http://dx.doi.org/10.1016/j.fuproc.2011.09.012.
[51] A.W. Marczewski, Application of mixed order rate equations to adsorption of methylene blue on mesoporous carbons, Appl. Surf. Sci. 256 (2010) 5145–5152, http://dx.doi.org/10.1016/j.apsusc.2009.12.078.
[52] M. Constantin, I. Asmarandei, V. Harabagiu, L. Ghimici, P. Ascenzi, G. Fundueanu, Removal of anionic dyes from aqueous solutions by an ion-exchanger based on pullulan microspheres, Carbohydr. Polym. 91 (2013) 74–84, http://dx.doi.org/10.1016/j.carbpol.2012.08.005.
[53] M.C. Ncibi, Applicability of some statistical tools to predict optimum adsorption isotherm after linear and non-linear regression analysis, J. Hazard. Mater. 153 (2008) 207–212, http://dx.doi.org/10.1016/j.jhazmat.2007.08.038.
[54] K.V. Kumar, K. Porkodi, F. Rocha, Isotherms and thermodynamics by linear and non-linear regression analysis for the sorption of methylene blue onto activated carbon: comparison of various error functions, J. Hazard. Mater. 151 (2008) 794–804, http://dx.doi.org/10.1016/j.jhazmat.2007.06.056.
[55] C. Cojocaru, M. Diaconu, I. Cretescu, J. Savic, V. Vasic, Biosorption of copper(II) ions from aqua solutions using dried yeast biomass, Colloids Surf. A Physicochem. Eng. Asp. 335 (2009) 181–188, http://dx.doi.org/10.1016/j.colsurfa.2008.11.003.
[56] K.V. Kumar, S. Sivanesan, Isotherm parameters for basic dyes onto activates carbon: comparision of linear and non-linear method, J. Hazard. Mater. 129 (2006) 147–150, http://dx.doi.org/10.1016/j.jhazmat.2005.08.022.
[57] N. Unlu, M. Ersoz, Removal of heavy metal ions by using dithiocarbamated-sporopollenin, Sep. Purif. Technol. 52 (2007) 461–469, http://dx.doi.org/10.1016/j.seppur.2006.05.026.
[58] L. Bulgariu, C. Cojocaru, B. Robu, M. Macoveanu, Equilibrium isotherms studies for sorption of lead ions from aqueous solutions using romanian peat sorbent, Environ. Eng. Manag. J. 6 (2007) 425–430.
[59] K.-W. Jung, B.H. Choi, M.-J. Hwang, T.-U. Jeong, K.-H. Ahn, Fabrication of granular activated carbons derived from spent coffee grounds by entrapment in calcium alginate beads for adsorption of acid orange 7 and methylene blue, Bioresour. Technol. 219 (2016) 185–195, http://dx.doi.org/10.1016/j.biortech.2016.07.098.
[60] R. Fabryanty, C. Valencia, F.E. Soetaredjo, J.N. Putro, S.P. Santoso, A. Kurniawan, Y.-H. Ju, S. Ismadji, Removal of crystal violet dye by adsorption using bentonite – alginate composite, J. Environ. Chem. Eng. 5 (2017) 5677–5687, http://dx.doi.org/10.1016/j.jece.2017.10.057.
[61] L. Yang, X. Ma, N. Guo, Sodium alginate/Na + -rectorite composite microspheres: preparation, characterization, and dye adsorption, Carbohydr. Polym. 90 (2012) 853–858, http://dx.doi.org/10.1016/j.carbpol.2012.06.011.
[62] O. Trott, A.J. Olson, AutoDock Vina: improving the speed and accuracy of docking with a new scoring function, efficient optimization, and multithreading, J. Comput. Chem. 31 (2010) 455–461, http://dx.doi.org/10.1002/jcc.21334.
[63] (a) M.M. Kuttel, Jonas Ståhle, Göran Widmalm, CarbBuilder: software for building molecular models of complex oligo- and polysaccharide structures, J. Comput. Chem. 37 (2016) 2098–2105, http://dx.doi.org/10.1002/jcc.24428;
(b) CarbBuilder web-site, Bioorganic Chemistry, The Widmalm Research Group, http://www.organ.su.se/gw/doku.php?id=CarbBuilder.
[64] E. Krieger, G. Koraimann, G. Vriend, Increasing the precision of comparative models with YASARA NOVA—a self-parameterizing force field, Proteins 47 (2002) 393–402, http://dx.doi.org/10.1002/prot.10104.